

Article

# Three New Lead Iodide Chain Compounds, APbI<sub>3</sub>, Templated by Molecular Cations

Yuan-Yuan Guo, Lin-Jie Yang and Philip Lightfoot \*

School of Chemistry and EaStChem, University of St Andrews, St Andrews KY16 9ST, UK; yg28@st-andrews.ac.uk (Y.G.); ly29@st-andrews.ac.uk (L.Y.)

\* Correspondence: pl@st-andrews.ac.uk; Tel.: +44-1334-463841

Received: 5 November 2019; Accepted: 21 November 2019; Published: 24 November 2019

**Abstract:** The crystal structures of three new hybrid organic-inorganic lead halide compounds [IqH]PbI<sub>3</sub>, [4MiH]PbI<sub>3</sub>, and [BzH]PbI<sub>3</sub> ([IqH<sup>+</sup>] = isoquinolinium, [4MiH<sup>+</sup>] = 4-methylimidazolium, [BzH<sup>+</sup>] = benzotriazolium) have been determined by single crystal x-ray diffraction. All three compounds have the same generic formula as perovskite, ABX<sub>3</sub>, but adopt a rare non-perovskite structure built from one dimensional (1D) edge-sharing octahedral chains. The bandgap of each compound was investigated by solid UV-Vis spectra. In comparison with previously reported hybrid compounds containing the same type of octahedral chains, [C<sub>10</sub>H<sub>7</sub>CH<sub>2</sub>NH<sub>3</sub>]PbI<sub>3</sub> and (C<sub>7</sub>H<sub>7</sub>N<sub>2</sub>)PbI<sub>3</sub>, all three new compounds have lower bandgaps (<2.4 eV), indicating that they may be promising for photovoltaic application.

**Keywords:** lead halides; hybrid perovskites; crystal structure

## 1. Introduction

The study of perovskite-related materials has grown tremendously in recent years [1] due to their enormous chemical and structural diversity and excellent physical properties, for example, ferroelectricity, luminescence, or magnetism [2–4]. In particular, lead(II) halide perovskites show impressive performances in their electronic and photophysical properties [5], making them promising candidates for practical applications such as solar cells [6,7] and light-emitting devices (LEDs) [8,9].  $\alpha$ -CsPbI<sub>3</sub>, for instance, exhibits a suitable bandgap ( $E_g = \sim 1.7$  eV), and is an excellent candidate for photovoltaic applications [10–12]. The general formula for perovskites is ABX<sub>3</sub>, where A is a large cation, B is a smaller cation, and X is an anion. However, there are many families of “perovskite-related” materials, which contain, for example, layered structural units derived from the archetypal “cubic” perovskite structure [5]. Conversely, not all ABX<sub>3</sub> compositions form perovskites, and several other structural architectures based on linked octahedral BX<sub>6</sub> units are available for such a stoichiometry, incorporating either face-sharing or edge-sharing rather than perovskite-like corner-sharing octahedra [13]. The simple composition CsPbI<sub>3</sub> adopts four different polymorphic forms:  $\alpha$ -CsPbI<sub>3</sub> (cubic),  $\beta$ -CsPbI<sub>3</sub> (tetragonal),  $\gamma$ -CsPbI<sub>3</sub> (orthorhombic), and  $\delta$ -CsPbI<sub>3</sub> (orthorhombic) [10,11,14]. The first three structures are ABX<sub>3</sub> “cubic” type perovskites ( $\alpha$  is aristotype cubic,  $\beta$ , and  $\gamma$  can be treated as lower symmetry, distorted structures due to “tilting” of the constituent octahedral PbI<sub>6</sub> units). Interestingly, the most stable ambient phase,  $\delta$ -CsPbI<sub>3</sub>, is a non-perovskite, which adopts a one dimensional (1D) edge-sharing octahedral chain structure type [15], similar to the known compounds NH<sub>4</sub>CdCl<sub>3</sub> [16] and RbPbI<sub>3</sub> [17,18] (Figure 1). Both the perovskite-structure polymorphs and non-perovskite phase play a significant role in better understanding the structure-property relationships amongst these different polymorphs. In contrast to the large variety of lead halide materials reported based on the cubic perovskite structure and its layered derivatives, here, we focused on developing the much less common 1D edge-sharing octahedral chain structure type, particularly in hybrid organic–inorganic lead halide materials. The only previous examples, to the

best of our knowledge, are  $[\text{C}_{10}\text{H}_7\text{CH}_2\text{NH}_3]\text{PbI}_3$  [19],  $(\text{C}_7\text{H}_7\text{N}_2)\text{PbI}_3$  [20], “ $(\text{ABT})_2[\text{PbBr}_3]$ ” [21], and  $(\text{ABT})[\text{PbCl}_3]$  [22].

Here, we represent three further examples of this rare structure type amongst hybrid organic–inorganic lead halide materials:  $[\text{IqH}]\text{PbI}_3$ ,  $[\text{4MiH}]\text{PbI}_3$ , and  $[\text{BzH}]\text{PbI}_3$ , ( $[\text{IqH}^+] = \text{isoquinolinium}$ ,  $[\text{4MiH}^+] = \text{4-methylimidazolium}$ , and  $[\text{BzH}^+] = \text{benzotriazolium}$ ). Single crystal x-ray diffraction experiments were performed to understand the structural variations of these three materials including structural distortions of the inorganic components and the nature of hydrogen bonding in directing the overall crystal packing. Furthermore, UV-Vis absorbance spectroscopy was carried out on powder samples of all three samples, and bandgaps were derived from Tauc-Plots [23].

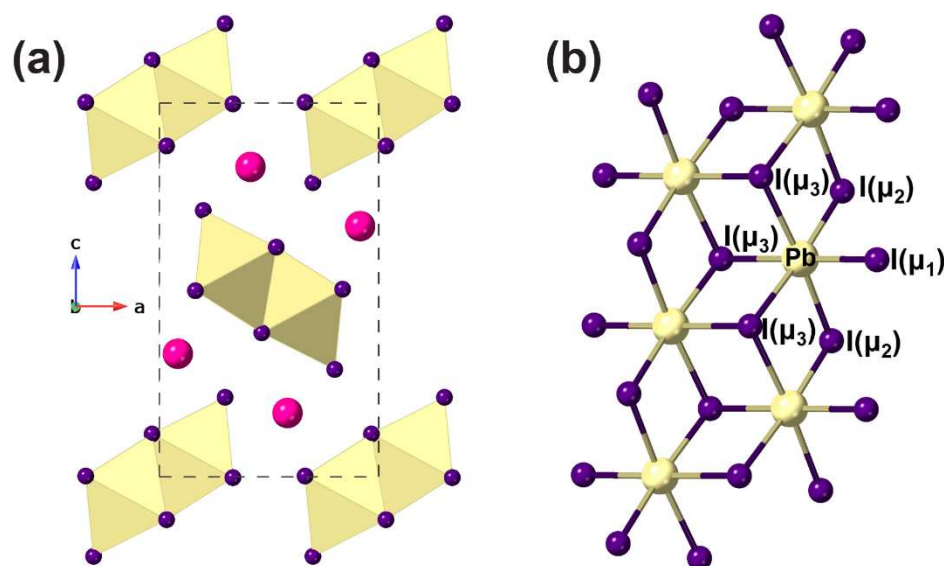


**Figure 1.** (a) Crystal structure of  $\delta\text{-CsPbI}_3$  viewed along the  $b$  axis. (b) 1D infinite double chain  $[\text{PbI}_3]_n$  formed by edge-linked  $\text{PbI}_6$  octahedra. Note that there are three types of iodine coordination: terminal ( $\mu_1$ ), doubly bridging ( $\mu_2$ ), and triply bridging ( $\mu_3$ ).

## 2. Experimental Section

### 2.1. Chemicals

Lead (II) iodide ( $\text{PbI}_2$ ,  $\geq 98\%$ ), hydroiodic acid (HI, 57%, w/w aqueous solution, stabilized with 1.5% hypophosphorous acid), isoquinoline ( $\text{C}_9\text{H}_7\text{N}$ , 97%), and 4-methylimidazole ( $\text{C}_4\text{H}_6\text{N}_2$ , 98%) were purchased from Alfa Aesar, Lancashire, UK. Benzotriazole ( $\text{C}_6\text{H}_5\text{N}_3$ , 99%) was purchased from Sigma Aldrich, Dorset, UK. All chemicals were directly used without further purification.

### 2.2. Synthesis

For  $[\text{IqH}]\text{PbI}_3$  ( $\text{C}_9\text{H}_8\text{NPbI}_3$ ), isoquinoline (0.18 mL, 1.5 mmol), and  $\text{PbI}_2$  (0.922 g, 1 mmol) were dissolved in conc. HI (12 mL) with moderate heating. By cooling for a few hours, yellow, needle-shaped crystals were obtained. These were filtered and washed with diethyl ether (yield 72.0% based on  $\text{PbI}_2$ ). The powder x-ray diffraction and Rietveld refinement are given in Figure S1. Elemental analysis: (anal. calc. (%)) for  $[\text{IqH}]\text{PbI}_3$ : C, 15.05; H, 1.12; N, 1.95. Found: C, 15.20; H, 1.08; N, 2.04).

For  $[\text{4MiH}]\text{PbI}_3$  ( $\text{C}_4\text{H}_7\text{N}_2\text{PbI}_3$ ), 4-methylimidazole (0.329 g, 4 mmol) and  $\text{PbI}_2$  (0.922 g, 2 mmol) were dissolved in conc. HI (8 mL) with moderate heating. By cooling for a few hours, yellow, needle-shaped crystals were obtained. These were filtered and washed with diethyl ether (yield 22.5% based on  $\text{PbI}_2$ ). The powder x-ray diffraction and Rietveld refinement are given in Figure S2. Elemental analysis: (anal. calc. (%)) for  $[\text{4MiH}]\text{PbI}_3$ : C, 7.16; H, 1.05; N, 4.17. Found: C, 7.17; H, 0.98; N, 4.12).

For  $[\text{BzH}]\text{PbI}_3$  ( $\text{C}_6\text{H}_6\text{N}_3\text{PbI}_3$ ), benzotriazole (0.476 g, 4 mmol) and  $\text{PbI}_2$  (0.922 g, 2 mmol) were dissolved in conc. HI (12 mL) with moderate heating. By cooling for a few hours, yellow, needle-shaped crystals were obtained. These were filtered and washed with diethyl ether (yield 47.2% based

on  $\text{PbI}_2$ ). The powder x-ray diffraction and Rietveld refinement are given in Figure S3. Elemental analysis: (anal. calc. (%)) for  $[\text{BzH}]\text{PbI}_3$ : C, 10.18; H, 0.85; N, 5.93. Found: C, 10.22; H, 0.80; N, 5.97).

### 2.3. Characterization

Single crystal X-ray diffraction data were collected at 173 K and 298 K on a Rigaku XtaLAB P200 diffractometer and a Rigaku SCX Mini diffractometer using  $\text{Mo-K}\alpha$  radiation (Rigaku, Houston, TX, USA). Data were collected using CrystalClear (Rigaku) software [24]. Structures were solved by direct methods using SHELXT [25], and full-matrix least-squares refinements on  $F^2$  were carried out using SHELXL-2018/3 [26] incorporated in the WINGX program [27]. Absorption corrections were performed empirically from equivalent reflections on the basis of multi-scans by using CrystalClear [24]. Non-H atoms were refined anisotropically and hydrogen atoms were treated as riding atoms. CrystalMaker [28] was used in preparing Figures 1–5. A Flack parameter of 0.357(5) for  $[\text{IqH}]\text{PbI}_3$  suggests an inversion twin component, but refinement of this did not significantly improve the fit.

Powder X-ray diffraction data were collected on a PANalytical EMPYREAN diffractometer using  $\text{Cu K}\alpha_1$  ( $\lambda = 1.5406 \text{ \AA}$ ) radiation in the range of 3 to  $70^\circ$  to confirm the purity of each sample (Malvern Panalytical, Ltd, Malvern, UK). Rietveld refinements were carried out using the GSAS package [29] with the EXPGUI interface [30].

Solid UV-Vis absorbance spectra were collected on a JASCO-V550 ultraviolet–visible spectrophotometer with the wavelength range at 200 nm to 900 nm (JASCO Corporation, Essex, UK).

## 3. Results and Discussion

Crystallographic details for the three new compounds are given in Table 1. Although single crystal X-ray data were collected at both 173 K and 298 K, there were only slight changes in molecular geometry between the two temperatures, with no phase changes detected in this temperature regime. The following discussion therefore refers to the structures at 173 K only, (details at 298 K are given in the Supplementary Materials). Each crystal structure exhibits the type of  $[\text{PbI}_3]_\infty$  chain found in  $\delta\text{-CsPbI}_3$  (Figure 1). This chain may be regarded as derived from the hexagonal, layered  $\text{PbI}_2$  structure by “stripping out” a double strand of condensed  $\text{PbI}_6$  octahedra from the  $\text{PbI}_2$  layer. This leads to one short unit cell axis of around  $4.6 \text{ \AA}$  for each of the crystal structures, which represents the Pb–Pb distance between two adjacent edge-shared octahedra. Within each  $[\text{PbI}_3]_\infty$  chain, there are three distinct types of iodide environment, designated as  $\mu_1$  (terminal),  $\mu_2$  (bridging two Pb centers), or  $\mu_3$  (bridging three Pb centers); these were designated as I1, I2, and I3, respectively, in each of the three new structures. This intrinsic asymmetry of the environment of both the  $\text{I}^-$  and  $\text{Pb}^{2+}$  environments leads to considerable distortions of the  $\text{PbI}_6$  octahedra, as detailed in Figure 2. For  $[\text{IqH}]\text{PbI}_3$ ,  $[\text{4MiH}]\text{PbI}_3$ , and  $[\text{BzH}]\text{PbI}_3$ , respectively, the Pb–I bond lengths were in the ranges of  $3.0063(6)$ – $3.5061(6)$ ,  $3.0329(5)$ – $3.4849(5)$ , and  $3.1197(7)$ – $3.3709(7) \text{ \AA}$ , the I–Pb–I bond angles in the ranges of  $85.582(14)$ – $95.198(16)$ ,  $82.133(13)$ – $95.401(14)$ , and  $84.807(17)$ – $99.555(18)^\circ$ , and the Pb–I–Pb bond angles in the ranges of  $91.303(15)$ – $92.714(15)$ ,  $87.357(14)$ – $92.440(13)$ , and  $87.953(17)$ – $94.323(16)^\circ$  at 173 K. The distortions were further quantified using conventional polyhedral distortion indices and compared to those of the previously known examples of hybrid compounds displaying the same type of  $[\text{PbI}_3]_\infty$  chain in Table 2. It is apparent that there is a considerable range of  $\Delta d$  and  $\sigma^2$  distortions amongst this family. For comparison, the two known inorganic analogues,  $\text{-CsPbI}_3$  and  $\text{RbPbI}_3$ , have  $\Delta d$  values of 10.61 and 8.81 and  $\sigma^2$  values of 19.0 and 20.6, respectively (Table S6). It is generally the case in these structures that a larger  $\Delta d$  corresponds to a smaller  $\sigma^2$ , but the detailed systematics and origins of the distortion behavior are not clear. There is, however, a clear trend in the amount of “underbonding” seen for the iodine sites in the  $[\text{PbI}_3]_\infty$  chain, which follows the order  $\text{I1} > \text{I2} > \text{I3}$  (see bond valence sums, Table 2). This lack of sufficient bonding for I1 in particular, despite the Pb–I1 bond being the shortest in each case, is compensated by I1 being a strong H-bond acceptor, a feature which presumably dictates the orientation of the organic cation relative to the inorganic chain in each case. This is especially seen in the case of  $[\text{BzH}]\text{PbI}_3$ , where I1 accepts two strong H-bonds (Table 3). Similar arguments and correlations can be seen in the behavior of the I2 and I3 sites by comparing the number and strength of H-bonds (Table 3) versus the corresponding iodine bond valence sums (Table 2).

**Table 1.** Crystal and structure refinement data for [IqH]PbI<sub>3</sub>, [4MiH]PbI<sub>3</sub>, and [BzH]PbI<sub>3</sub> at 173 K.

Compound	[IqH]PbI <sub>3</sub>	[4MiH]PbI <sub>3</sub>	[BzH]PbI <sub>3</sub>
Formula	C <sub>9</sub> NH <sub>8</sub> PbI <sub>3</sub>	C <sub>4</sub> N <sub>2</sub> H <sub>7</sub> PbI <sub>3</sub>	C <sub>6</sub> N <sub>3</sub> H <sub>6</sub> PbI <sub>3</sub>
Formula Weight	718.05	671.01	708.03
Crystal System	Orthorhombic	Monoclinic	Orthorhombic
Space Group	<i>P</i> 2 <sub>1</sub> 2 <sub>1</sub> 2 <sub>1</sub>	<i>P</i> 2 <sub>1</sub> / <i>c</i>	<i>P</i> 2 <sub>1</sub> 2 <sub>1</sub> 2 <sub>1</sub>
<i>a</i> /Å	4.6946(2)	4.6110(2)	4.6102(2)
<i>b</i> /Å	12.8898(9)	22.2560(16)	12.4712(9)
<i>c</i> /Å	23.2093(16)	11.7926(8)	22.2047(16)
$\beta$ /°	-	98.801(9)	-
<i>V</i> /Å <sup>3</sup>	1404.45(15)	1195.94(13)	1276.65(14)
<i>Z</i>	4	4	4
MEASURED Ref	11890	12122	13081
Independent Ref	2473	2717	2893
GOOF	[R(int) = 0.0399]	[R(int) = 0.0631]	[R(int) = 0.0556]
Final R Indices ( <i>I</i> > 2σ( <i>I</i> ))	R <sub>1</sub> = 0.0187 wR <sub>2</sub> = 0.0399	R <sub>1</sub> = 0.0272 wR <sub>2</sub> = 0.0544	R <sub>1</sub> = 0.0207 wR <sub>2</sub> = 0.0373
Flack Parameter	0.357(5)		0.006(5)

**Table 2.** Calculated bond length distortions <sup>§</sup> and bond angle variance <sup>§</sup> and bond valence sums <sup>£</sup> for [IqH]PbI<sub>3</sub>, [4MiH]PbI<sub>3</sub>, and [BzH]PbI<sub>3</sub> at 173 K, and previously reported [C<sub>10</sub>H<sub>7</sub>CH<sub>2</sub>NH<sub>3</sub>]PbI<sub>3</sub> (298 K) and (C<sub>7</sub>H<sub>7</sub>N<sub>2</sub>)PbI<sub>3</sub> (173 K).

Compound	[IqH]PbI <sub>3</sub>	[4MiH]PbI <sub>3</sub>	[BzH]PbI <sub>3</sub>	[C <sub>10</sub> H <sub>7</sub> CH <sub>2</sub> NH <sub>3</sub> ]PbI <sub>3</sub> [19]	(C <sub>7</sub> H <sub>7</sub> N <sub>2</sub> )PbI <sub>3</sub> [20]
$\Delta d$ (× 10 <sup>-4</sup> )	21.30	17.32	9.34	18.68	8.34
$\sigma^2$	10.70	13.88	16.66	9.92	12.38
$\Sigma v$ (Pb)	1.82	1.86	1.79	1.80	1.78
$\Sigma v$ (I1)	0.54	0.50	0.40	0.54	0.42
$\Sigma v$ (I2)	0.56	0.66	0.70	0.48	0.64
$\Sigma v$ (I3)	0.71	0.70	0.68	0.78	0.72

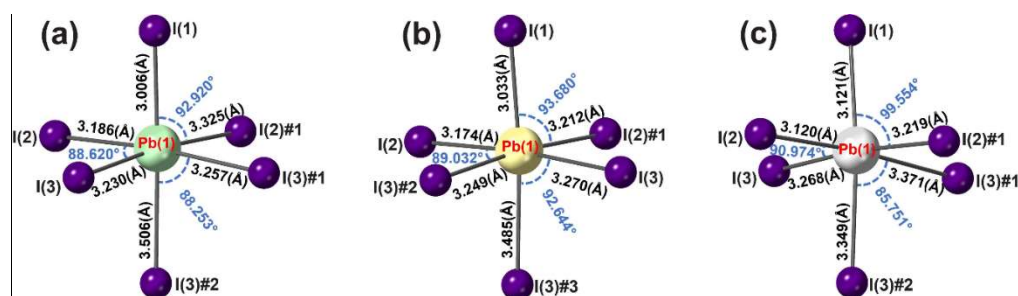
$$\Delta d = \left(\frac{1}{6}\right) \sum \left[\frac{d_n - d}{d}\right]^2 \quad \text{Equation (1)}$$

$$\sigma^2 = \sum_{i=1}^{12} \frac{(\theta_i - 90)^2}{11} \quad \text{Equation (2)}$$

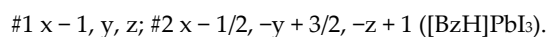
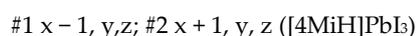
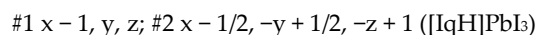
$$v_{ij} = \exp\left(\frac{R_0 - d}{b}\right) \quad \text{Equation (3)}$$

<sup>§</sup> The bond length distortion of the octahedra in each composition at both 173 and 298 K was calculated using Equation (1) [31], where *d* is the average Pb–I bond distance and *d<sub>n</sub>* are the six individual bond distances. The bond angle variance of each octahedron from the ideal 90° of an undistorted structure was calculated using Equation (2) [32], where  $\theta_i$  is the individual I–Pb–I angle.

<sup>£</sup> The bond valence was calculated using Equation (3) [33], where *d* is the individual bond length, *R*<sub>0</sub> is a constant for a particular bond type, here *R*<sub>0</sub> = 2.78 Å for the Pb–I bond, and *b* = 0.37 Å, a universal constant. The bond valence sum,  $\Sigma v_i$ , is the summation of the individual bond valences:

**Figure 2.** The nature of the distortion within the PbI<sub>6</sub> octahedra in (a) [IqH]PbI<sub>3</sub>, (b) [4MiH]PbI<sub>3</sub>, and (c) [BzH]PbI<sub>3</sub>, at 173 K. In each case, there is only one crystallographically unique Pb site, and three I

sites:  $\mu_1$  (terminal),  $\mu_2$  (bridging two Pb centers), or  $\mu_3$  (triple bridging); these were designated as I1, I2, and I3, respectively.



Hence, the overall crystal packing is dictated by the nature of the *inter-chain* interactions, mediated by hydrogen bonds from the molecular cations. Details of H-bonding are shown in Table 3. However, despite the quite distinct nature of the molecular cations, in terms of size, shape, and H-bonding options, each of the structures adopts a similar relative packing of the inorganic chains, which results in quite similar unit cell metrics (Table 1) and is shown in more detail in Figures 3–5. Moreover, the space group symmetries for [IqH]PbI<sub>3</sub> and [BzH]PbI<sub>3</sub> are the same, and, in this sense, these two may be regarded as isostructural, although in the former case each organic moiety has only one H-bond donor atom and hydrogen-bonds to only one adjacent inorganic chain, whereas in the latter, the corresponding moiety bridges two adjacent chains via two distinct H-bond donor atoms. The symmetry of [4MiH]PbI<sub>3</sub> differs, exhibiting more subtle distortions due to the enhanced effects of the *inter-chain* interactions, whereby each organic moiety bridges three adjacent inorganic chains via the two H-bond donors. This leads to a slightly different displacement of adjacent [PbI<sub>3</sub>]<sub>∞</sub> chains, such that the shortest *inter-chain* I–I distance in [4MiH]PbI<sub>3</sub> is 4.23 Å, compared to 4.31 Å in  $\delta$ -CsPbI<sub>3</sub> [11] 4.72 Å in [IqH]PbI<sub>3</sub> and 4.39 Å in [BzH]PbI<sub>3</sub>.

It is of interest to compare the crystal packing within these three new examples to those of the two previously known examples. (C<sub>7</sub>H<sub>7</sub>N<sub>2</sub>)PbI<sub>3</sub> [20] is essentially isostructural with [IqH]PbI<sub>3</sub> and [BzH]PbI<sub>3</sub>, with the same space group and similar unit cell metrics. Indeed, the H-bonding scheme also very closely mimics that in [BzH]PbI<sub>3</sub>. The organic moiety in (C<sub>7</sub>H<sub>7</sub>N<sub>2</sub>)PbI<sub>3</sub> is benzimidazolium, which differs from benzotriazolium only in the substitution of the ‘central’ N atom by C–H. This minor change to a ‘hydrogen-bond-inactive’ part of the molecule clearly does not influence the crystal packing. In contrast, [C<sub>10</sub>H<sub>7</sub>CH<sub>2</sub>NH<sub>3</sub>]PbI<sub>3</sub> [19] contains 1-naphthylmethylamine, which has more limited H-bonding opportunities, leading to a quite different style of crystal packing to those observed here.

**Table 3.** Hydrogen bonds for [IqH]PbI<sub>3</sub>, [4MiH]PbI<sub>3</sub>, and [BzH]PbI<sub>3</sub> at 173 K (Å and °).

Compound	D–H...A	d(D–H)	d(H...A)	d(D...A)	<(DHA)
[IqH]PbI <sub>3</sub>	N(1)–H(1)...I(1)	0.86	3.24	3.852(7)	130.0
	N(1)–H(1)...I(2)	0.86	2.94	3.626(7)	138.3
	N(1)–H(1)...I(2)	0.86	3.04	3.612(7)	126.3
[4MiH]PbI <sub>3</sub>	N(1)–H(1)...I(1)#4	0.86	3.07	3.812(6)	145.2
	N(2)–H(2)...I(1)#5	0.86	2.96	3.700(7)	145.2
[BzH]PbI <sub>3</sub>	N(1)–H(1)...I(1)#5	0.86	2.90	3.598(7)	139.1
	N(3)–H(2)...I(1)	0.86	2.79	3.490(7)	139.2

Symmetry transformations used to generate equivalent atoms: #4  $x, -y + 1/2, z - 1/2$ ; #5  $x + 1, y, z - 1$  ([4MiH]PbI<sub>3</sub>). #5  $-x + 1, y + 1/2, -z + 3/2$  ([BzH]PbI<sub>3</sub>).

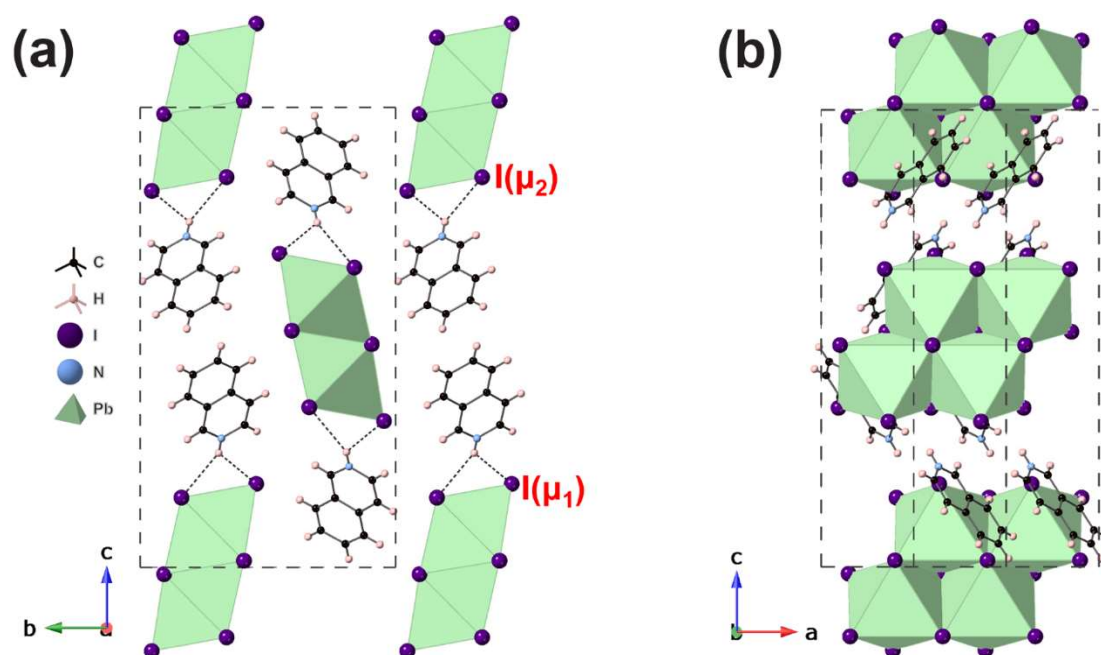


**Figure 3.** Unit cell packing and hydrogen-bonding scheme for [IqH]PbI<sub>3</sub> (a) along the *a*-axis and (b) along the *b* axis.

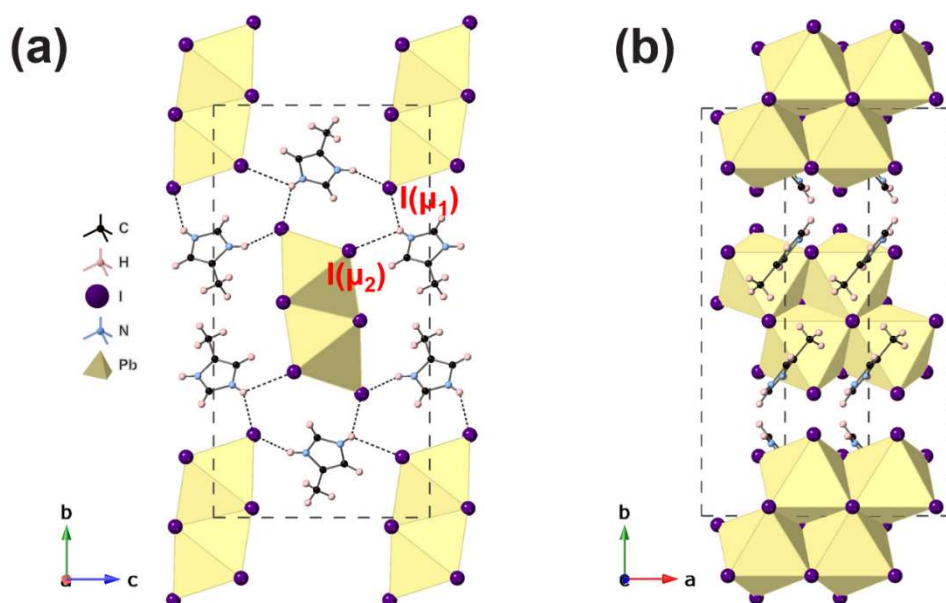


**Figure 4.** Unit cell packing and hydrogen-bonding scheme for [4MiH]PbI<sub>3</sub> (a) along the *a*-axis and (b) along the *c* axis.

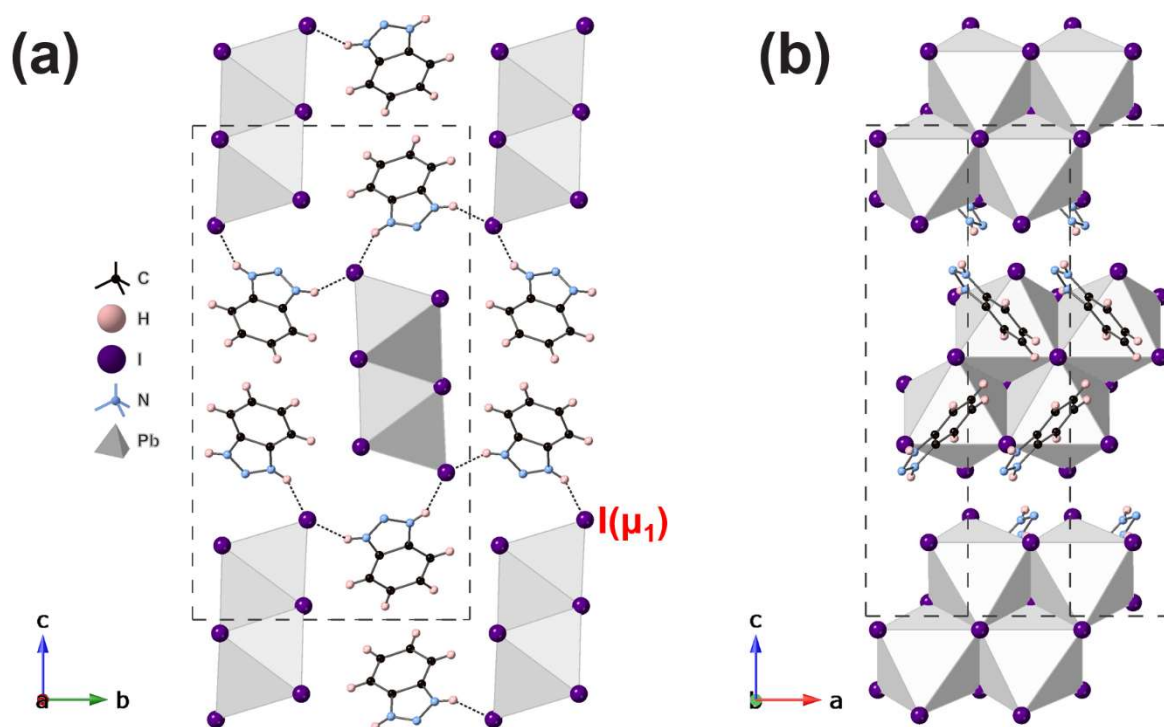


**Figure 5.** Unit cell packing and hydrogen-bonding scheme for [BzH]PbI<sub>3</sub> (a) along the *a*-axis and (b) along the *b* axis.

UV–Vis absorbance spectra were carried out for all three powder samples: [IqH]PbI<sub>3</sub>, [4MiH]PbI<sub>3</sub>, and [BzH]PbI<sub>3</sub> at wavelengths between 200 nm to 900 nm (Figure 6). The absorption spectra revealed that all three compounds featured similar peaks at ~385 nm (3.2 eV) and ~415 nm (3.0 eV). Interestingly, [BzH]PbI<sub>3</sub> has an extra absorption peak at ~493 nm (2.5 eV), leading to a band gap significantly lower than the other two, as derived from the Tauc-Plot (inset Figure 6). The derived band gaps were 2.36 eV, 2.28 eV, and 2.16 eV for [IqH]PbI<sub>3</sub>, [4MiH]PbI<sub>3</sub>, and [BzH]PbI<sub>3</sub>, respectively. It can be noted that the band gaps of all three new compounds we report here are lower than the two known examples of the same structure type: [C<sub>10</sub>H<sub>7</sub>CH<sub>2</sub>NH<sub>3</sub>]PbI<sub>3</sub> (absorption peak is at ~401 nm) [19], and (C<sub>7</sub>H<sub>7</sub>N<sub>2</sub>)PbI<sub>3</sub> (band gap is E<sub>g</sub> = 2.44 eV) [20].

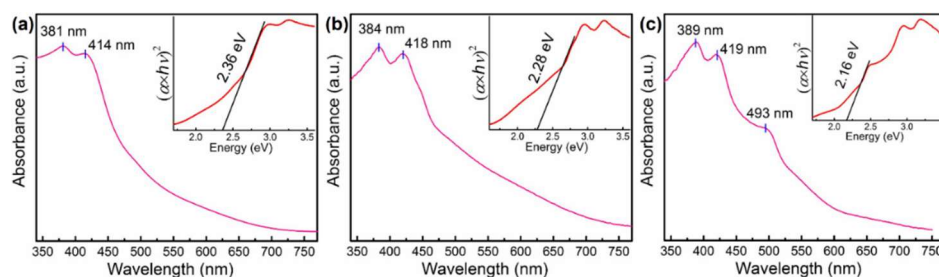


**Figure 6.** UV absorption spectra and Tauc-Plot (inset) of (a) [IqH]PbI<sub>3</sub>, (b) [4MiH]PbI<sub>3</sub>, and (c) [BzH]PbI<sub>3</sub> at room temperature.

#### 4. Conclusions

In conclusion, we have prepared three new examples of an unusual [PbI<sub>3</sub>]<sub>∞</sub> chain consisting of edge-shared PbI<sub>6</sub> octahedra. This type of chain has been previously seen only rarely in both inorganic and hybrid lead halides. Structural distortions within the [PbI<sub>3</sub>]<sub>∞</sub> chains, and the crystal packing of the chains themselves, can be rationalized to some extent, based on the hydrogen-bonding requirements of the organic moieties. However, the contrasting nature of the three amines used here suggests that structural and compositional features of molecular ‘templates’ that might direct the

crystallization of this type of  $[\text{PbI}_3]_\infty$  chain, and thus favor the crystallization of these structure types rather than competing  $\text{APbI}_3$  (or other) polymorphs, may be difficult to predict. Further work is merited in exploring related examples of organic amines.

**Supplementary Materials:** The following are available online at [www.mdpi.com/2073-4352/9/12/616/s1](http://www.mdpi.com/2073-4352/9/12/616/s1), Figures S1–S3: Rietveld refinements of powder X-ray diffraction data; Table S1: Crystallographic data for all three compounds at 298 K; Tables S2–S4: Selected bond lengths and angles versus temperature for all three compounds; Table S5: Hydrogen bonds; Table S6: distortion parameters for  $\delta$ - $\text{CsPbI}_3$  and  $\text{RbPbI}_3$  at 298 K.

**Author Contributions:** Y.G. and L.Y. carried out all the chemistry, crystallography. and further characterization. P.L. coordinated the project and writing of the paper, with the approval of all authors.

**Funding:** This research was funded by the China Scholarship Council, grant number 201603780005" the University of St Andrews. Raw data pertaining to this work are available at <https://doi.org/10.17630/bb979bce-5a77-45cf-b0c4-dfa7bd5c4588>.

**Conflicts of Interest:** The authors declare no conflicts of interest.

## References

1. Goesten, M.G.; Hoffmann, R. Mirrors of Bonding in Metal Halide Perovskites. *J. Am. Chem. Soc.* **2018**, *140*, 12996–13010.
2. Clulow, R.; Bradford, A.; Lee, S.; Lightfoot, P. Perovzalates: a family of perovskite-related oxalates. *Dalton Trans.* **2019**, 14461–14466.
3. Li, T.; Clulow, R.; Bradford, A.J.; Lee, S.L.; Slawin, A.M.Z.; Lightfoot, P. A hybrid fluoride layered perovskite,  $(\text{enH}_2)\text{MnF}_4$ . *Dalton Trans.* **2019**, *48*, 4784–4787.
4. Guo, Y.-Y.; McNulty, J.A.; Mica, N.A.; Samuel, I.D.W.; Slawin, A.M.Z.; Bühl, M.; Lightfoot, P. Structure-directing effects in (110)-layered hybrid perovskites containing two distinct organic moieties. *Chem. Commun.* **2019**, *55*, 9935–9938.
5. Saparov, B.; Mitzi, D.B. Organic-Inorganic Perovskites: Structural Versatility for Functional Materials Design. *Chem. Rev.* **2016**, *116*, 4558–4596.
6. Tsai, H.; Nie, W.; Blancon, J.C.; Stoumpos, C.C.; Asadpour, R.; Harutyunyan, B.; Neukirch, A.J.; Verduzco, R.; Crochet, J.J.; Tretiak, S.; et al. High-efficiency two-dimensional ruddlesden-popper perovskite solar cells. *Nature* **2016**, *536*, 312–317.
7. Li, X.; Hoffman, J.; Ke, W.; Chen, M.; Tsai, H.; Nie, W.; Mohite, A.D.; Kepenekian, M.; Katan, C.; Even, J.; et al. Two-Dimensional Halide Perovskites Incorporating Straight Chain Symmetric Diammonium Ions,  $(\text{NH}_3\text{C}_m\text{H}_{2m}\text{NH}_3)(\text{CH}_3\text{NH}_3)_{n-1}\text{PbnI}_{3n+1}$  ( $m = 4-9$ ;  $n = 1-4$ ). *J. Am. Chem. Soc.* **2018**, *140*, 12226–12238.
8. Gautier, R.; Massuyeau, F.; Galnon, G.; Paris, M. Lead Halide Post-Perovskite-Type Chains for High-Efficiency White-Light Emission. *Adv. Mater.* **2019**, *31*, 6–11.
9. Protesescu, L.; Yakunin, S.; Bodnarchuk, M.I.; Bertolotti, F.; Masciocchi, N.; Guagliardi, A.; Kovalenko, M. V. Monodisperse Formamidinium Lead Bromide Nanocrystals with Bright and Stable Green Photoluminescence. *J. Am. Chem. Soc.* **2016**, *138*, 14202–14205.
10. Steele, J.A.; Jin, H.; Dovgaliuk, I.; Berger, R.F.; Braeckevelt, T.; Yuan, H.; Martin, C.; Solano, E.; Lejaeghere, K.; Rogge, S.M.J.; et al. Thermal unequilibrium of strained black  $\text{CsPbI}_3$  thin films. *Science* **2019**, *365*, 679–684.
11. Straus, D.B.; Guo, S.; Cava, R.J. Kinetically Stable Single Crystals of Perovskite-Phase  $\text{CsPbI}_3$ . *J. Am. Chem. Soc.* **2019**, *141*, 11435–11439.
12. Zhao, B.; Jin, S.F.; Huang, S.; Liu, N.; Ma, J.Y.; Xue, D.J.; Han, Q.; Ding, J.; Ge, Q.Q.; Feng, Y.; et al. Thermodynamically Stable Orthorhombic  $\gamma$ - $\text{CsPbI}_3$  Thin Films for High-Performance Photovoltaics. *J. Am. Chem. Soc.* **2018**, *140*, 11716–11725.
13. Wu, L.M.; Wu, X.T.; Chen, L. Structural overview and structure-property relationships of iodoplumbate and iodobismuthate. *Coord. Chem. Rev.* **2009**, *253*, 2787–2804.
14. Trots, D.M.; Myagkota, S. V. High-temperature structural evolution of caesium and rubidium triiodoplumbates. *J. Phys. Chem. Solids* **2008**, *69*, 2520–2526.
15. Schelhas, L.T.; Li, Z.; Christians, J.A.; Goyal, A.; Kairys, P.; Harvey, S.P.; Kim, D.H.; Stone, K.H.; Luther, J.M.; Zhu, K.; et al. Insights into operational stability and processing of halide perovskite active layers. *Energy Environ. Sci.* **2019**, *12*, 1341–1348.

16. Rolies, M.M.; De Ranter, C.J. A new investigation of ammonium cadmium chloride. *Acta Crystallogr. Sect. B Struct. Crystallogr. Cryst. Chem.* **1978**, *34*, 3057–3059.
17. Saliba, M.; Matsui, T.; Domanski, K.; Seo, J.Y.; Ummadisingu, A.; Zakeeruddin, S.M.; Correa-Baena, J.P.; Tress, W.R.; Abate, A.; Hagfeldt, A.; et al. Incorporation of rubidium cations into perovskite solar cells improves photovoltaic performance. *Science* **2016**, *354*, 206–209.
18. Jung, M.H.; Rhim, S.H.; Moon, D. TiO<sub>2</sub>/RbPbI<sub>3</sub> halide perovskite solar cells. *Sol. Energy Mater. Sol. Cells* **2017**, *172*, 44–54.
19. Papavassiliou, G.C.; Mousdis, G.A.; Raptopoulou, C.P.; Terzis, A. Preparation and Characterization of [C<sub>6</sub>H<sub>5</sub>CH<sub>2</sub>NH<sub>3</sub>]<sub>2</sub>PbI<sub>4</sub>, [C<sub>6</sub>H<sub>5</sub>CH<sub>2</sub>CH<sub>2</sub>SC(NH<sub>2</sub>)<sub>2</sub>]<sub>3</sub>PbI<sub>5</sub> and [C<sub>10</sub>H<sub>7</sub>CH<sub>2</sub>NH<sub>3</sub>]<sub>3</sub>PbI<sub>3</sub> Organic-Inorganic Hybrid Compounds. *Z. Naturforsch* **1999**, *54b*, 1405–1409.
20. Lermer, C.; Harm, S.P.; Birkhold, S.T.; Jaser, J.A.; Kutz, C.M.; Mayer, P.; Schmidt-Mende, L.; Lotsch, B. V. Benzimidazolium Lead Halide Perovskites: Effects of Anion Substitution and Dimensionality on the Bandgap. *Zeitschrift fur Anorg. und Allg. Chemie* **2016**, *642*, 1369–1376.
21. Samet, A.; Triki, S.; Abid, Y. Resonantly Enhanced White-Light Emission Involving Energy and Charge Transfer in One-Dimensional Hybrid Material: (ABT)<sub>2</sub>[PbBr<sub>3</sub>]. *J. Phys. Chem. C* **2019**, *123*, 6213–6219.
22. Medhioub, O.; Barkaoui, H.; Samet, A.; Pillet, S.; Triki, S.; Abid, Y. Blue Emission from Charge-Transfer Excitons in Hybrid Organic-Inorganic Quantum Wires: (ABT)[PbCl<sub>3</sub>]. *J. Phys. Chem. C* **2019**, *123*, 26547–26553.
23. Tauc, J. Optical properties and electronic structure of amorphous Ge and Si. *Mater. Res. Bull.* **1968**, *3*, 37–46.
24. Rigaku. *CrystalClear*; Rigaku Corporation: Tokyo, Japan, 2014.
25. Sheldrick, G.M. SHELXT—Integrated space-group and crystal-structure determination. *Acta Crystallogr. Sect. A Found. Crystallogr.* **2015**, *71*, 3–8.
26. Sheldrick, G.M. Crystal structure refinement with SHELXL. *Acta Crystallogr. Sect. C Struct. Chem.* **2015**, *71*, 3–8.
27. Farrugia, L.J. WinGX and ORTEP for Windows: An update. *J. Appl. Cryst.* **2012**, *45*, 849–854.
28. Palmer, D. C. *CrystalMaker*; Agilent Technologies Ltd.: Yarnton, Oxfordshire, UK, 2014.
29. Larson, A.C.; Von Dreele, R.B. *General Structure Analysis System (GSAS)*; 1994; Los Alamos National Laboratory Report No. 88-748; Los Alamos National Laboratory: Los Alamos, NM, USA, 1994.
30. Toby, B.H. EXPGUI, a graphical user interface for GSAS. *J. Appl. Cryst.* **2001**, *34*, 210–213.
31. Lufaso, M.W.; Woodward, P.M. Jahn-Teller distortions, cation ordering and octahedral tilting in perovskites. *Acta Crystallogr. Sect. B Struct. Sci.* **2004**, *60*, 10–20.
32. Robinson, K.; Gibbs, G. V.; Ribbe, P.H. Quadratic Elongation: A Quantitative Measure of Distortion in Coordination Polyhedra. *Science* **1971**, *172*, 567–570.
33. Brese, N.E.; O’Keeffe, M. Bond-valence parameters for solids. *Acta Cryst. B* **1991**, *47*, 192–197.



© 2019 by the authors. Licensee MDPI, Basel, Switzerland. This article is an open access article distributed under the terms and conditions of the Creative Commons Attribution (CC BY) license (<http://creativecommons.org/licenses/by/4.0/>).